

# Charge transfer and x-ray emission reactions involving highly charged ions and neutral hydrogen

J A Perez<sup>1</sup>, R E Olson<sup>1</sup> and P Beiersdorfer<sup>2</sup>

<sup>1</sup> Department of Physics, University of Missouri-Rolla, Rolla, MO 65409-0640, USA

<sup>2</sup> Department of Physics and Advanced Space Technology,  
Lawrence Livermore National Laboratory, 7000 East Avenue, Livermore, CA 94551, USA

Received 14 December 2000, in final form 26 April 2001

Published 23 July 2001

Online at [stacks.iop.org/JPhysB/34/3063](http://stacks.iop.org/JPhysB/34/3063)

## Abstract

A three-body classical trajectory Monte Carlo method is used to study charge transfer between highly charged bare ions ( $\text{Ne}^{10+}$ ,  $\text{Ar}^{18+}$ ,  $\text{Fe}^{26+}$ ,  $\text{Kr}^{36+}$  and  $\text{Xe}^{54+}$ ) and neutral hydrogen at collision energies between  $1 \text{ eV amu}^{-1}$  and  $100 \text{ keV amu}^{-1}$ . The x-ray emission resulting from these reactions can be used as a diagnostic tool to study the charge transfer processes occurring in plasmas. For low-energy collisions ( $<100 \text{ eV amu}^{-1}$ ), the electrons are captured into states characterized by large principal quantum numbers and low angular momentum. A result of this non-statistical behaviour is the increase in Lyman series x-rays being emitted by captured electrons moving directly from high- $n$  states to the K-shell. Calculated results for the enhancement of K-shell x-ray emission at low energies compare favourably with measurements made at the Lawrence Livermore National Laboratory using the electron beam ion traps EBIT-II and SuperEBIT.

## 1. Introduction

Charge transfer reactions between highly charged ions and neutral atoms are of interest to researchers trying to understand line emissions produced in laboratory plasmas and more recently, in non-terrestrial sources such as comets [1]. In a laboratory plasma, such as found in the Joint European Torus (JET), Tokamak Fusion Test Reactor (TFTR) or the DIII-D tokamak, ions in the plasma interact with neutral beams pumped into the plasma and with the neutrals in the outer region of the plasma near the walls. The resulting charge transfer process leads to line emissions that can be used as a diagnostic tool to measure various parameters of a plasma such as temperature, velocity, electron density and the charge states of the ions present [2, 3]. In a tokamak plasma the line emissions of interest for diagnostics are usually found in the visible spectrum due to the need to perform remote sensing at the fusion reactor.

In non-terrestrial sources such as comets or solar flares, x-ray emissions are well suited for diagnostic use. X-rays can travel through circumstellar material, or in the case of large

distances, interstellar material, with less absorption occurring. The newly observed x-ray emissions emanating from comets are thought to arise from collisions between highly charged ions in the solar wind and neutral gases in the coma [4]. Collision energies range from around 3500 eV amu<sup>-1</sup> at the edge of the coma to less than 50 eV amu<sup>-1</sup> behind the bow shock region. The solar wind contains an abundance of heavy ion species such as Fe, that are highly charged. The cometary neutrals include H<sub>2</sub>O, OH, H and O.

Electrons captured by highly charged ions tend to occupy states characterized by high principal quantum numbers ( $n \gg 1$ ). Calculations have shown that the captured electrons tend to populate states according to

$$n_f = n_i \left( \frac{q}{Z} \right)^{3/4} \quad (1)$$

where  $n_f$  and  $n_i$  are the final and initial principal quantum numbers and  $q$  and  $Z$  are the projectile ion and neutral target core charges, respectively [5]. For atomic hydrogen, this leads to  $n_f = n_i q^{3/4}$ .

It is statistically more likely that capture into a high principal quantum number state also results in the electron having a large angular momentum since the population is weighted by the  $2l + 1$  degeneracy. In that case de-excitation occurs by a series of transitions with small changes in the principal quantum number ( $\Delta n = 1$ ). The dipole selection rules allow only transitions where the angular momentum quantum number,  $l$ , changes by 1.

If the ion has an open K-shell, de-excitation may occur by transitions with small changes in  $n$  and  $l$  until the electron reaches the  $n = 2, l = 1$  state whereby it can make the transition to the  $n = 1, l = 0$  state producing a Lyman- $\alpha$  x-ray. However, higher energy x-rays may be emitted by electron transitions to the K-shell from higher  $n$  states if the electron is captured into a state with low angular momentum which then cascades to an  $l = 1$  state with  $n > 2$ . The electron can also be directly captured into a high- $n$  state with  $l = 1$  resulting in a K-shell transition directly from the high- $n$  state (prompt x-ray emission). K-shell x-ray emission following charge transfer can be studied experimentally under controlled conditions using the EBIT-II and SuperEBIT electron beam ion traps at Lawrence Livermore National Laboratory. Calculations of the  $n$  and  $l$  values of the captured electrons are critical to the understanding of the observed x-ray emission.

In this work we use a three-body classical trajectory Monte Carlo (CTMC) method to study electron capture from hydrogen by highly charged-bare ions ( $A^{q+}$ ,  $q = 10, 18, 26, 36$  and  $54$ ). The total capture cross sections as well as state-selective capture cross sections are calculated for a wide range of collision energies. Using the state-selective capture cross sections, emission cross sections are calculated. Results for the ratio of prompt x-rays emitted to the Lyman- $\alpha$  transitions are given.

## 2. Method

The use of the CTMC method to describe collisions between highly charged ions and neutral atoms has been well documented and extensively benchmarked against experimental data [6]. In the CTMC method, a Hamiltonian for the system is set up and Hamilton's equations of motion are solved numerically to produce the trajectory of each particle. Thousands of collisions are simulated so that proper statistics can be obtained.

In this work the system consists of a projectile ion, electron and hydrogen nucleus. The Coulomb force is included between all particles in the system. The hydrogen atom is described by a microcanonical ensemble of the classical electron momentum and position phase space. This results in a classical momentum distribution for the electron that is the same as the

quantum distribution. The radial distribution in this case is not correct at large distances from the nucleus. However, it has been determined that this does not have a serious effect on capture collisions.

Once the electron has been captured by the projectile ion, the binding energy  $E$  is calculated, with  $E$  being the total energy of the electron with respect to the projectile ion. A classical principal quantum number is then calculated,

$$n_c = q/\sqrt{(2U)} \quad (2)$$

where  $U = |E|$ , and  $q$  is the charge of the projectile ion. This classical number is then assigned a principal quantum number such that the relationship

$$\left[(n-1)\left(n-\frac{1}{2}\right)n\right]^{1/3} \leq n_c \leq \left[n\left(n+\frac{1}{2}\right)(n+1)\right]^{1/3} \quad (3)$$

derived by Mackellar and Becker [7], is satisfied.

The classical orbital angular momentum is given by

$$l_c = [(x\dot{y} - y\dot{x})^2 + (x\dot{z} - z\dot{x})^2 + (y\dot{z} - z\dot{y})^2]^{1/2} \quad (4)$$

where  $x$ ,  $y$  and  $z$  are the Cartesian coordinates relative to the projectile nucleus. This classical number is then multiplied by a normalization factor of  $n/n_c$  that reflects that it is a non-integer number. Then an orbital angular momentum quantum number is assigned to this classical number according to the relationship

$$l \leq l_c \leq l+1. \quad (5)$$

This reproduces the correct  $2l+1$  quantal statistical distributions since  $l_c^2$  is uniformly distributed for a given  $n$  value [8].

Capture cross sections are calculated using

$$\sigma = \left(\frac{N}{N_{\text{total}}}\right) \pi b_{\text{max}}^2 \quad (6)$$

where  $N$  is the number of capture events,  $N_{\text{total}}$  is the total number of simulated collisions and  $b_{\text{max}}$  is the largest value for the impact parameter that will lead to a capture event.

### 3. Results

The collision energies ranged from 1 eV amu<sup>-1</sup> to 100 keV amu<sup>-1</sup>. In figure 1 the calculated total capture cross sections along with the cross sections for capture into a specific  $n$  state are plotted for the projectile ions used in this work. At low energies the largest contributions to the total capture cross sections come from capture into just one or two  $n$  states. In figure 1(a) we see that at energies <100 eV amu<sup>-1</sup>, virtually all electrons captured by Ne<sup>10+</sup> go into the  $n = 6$  state. For Fe<sup>26+</sup> (figure 1(c)), at low energies the major contributions to the total capture cross section comes from capture into the  $n = 11$  and 12 states. Likewise for Kr<sup>36+</sup> (figure 1(d)), capture into the  $n = 15$  and 16 states together contribute more than 85% to the total cross section. For Xe<sup>54+</sup> (figure 1(e)), the  $n = 21$  and 22 states are populated at collision energies <100 eV amu<sup>-1</sup>. The final  $n$  levels are in accord with the  $n_f = n_i q^{3/4}$  scaling relationship. In the energy range between 10 eV amu<sup>-1</sup> and 1 keV amu<sup>-1</sup>, only one  $n$  state is a major contributor to the total capture cross section for projectiles with initial charge states  $q \leq 18$  (figures 1(a) and (b)). At the higher energies the  $n$ -state capture cross sections become more evenly distributed for all the ions.

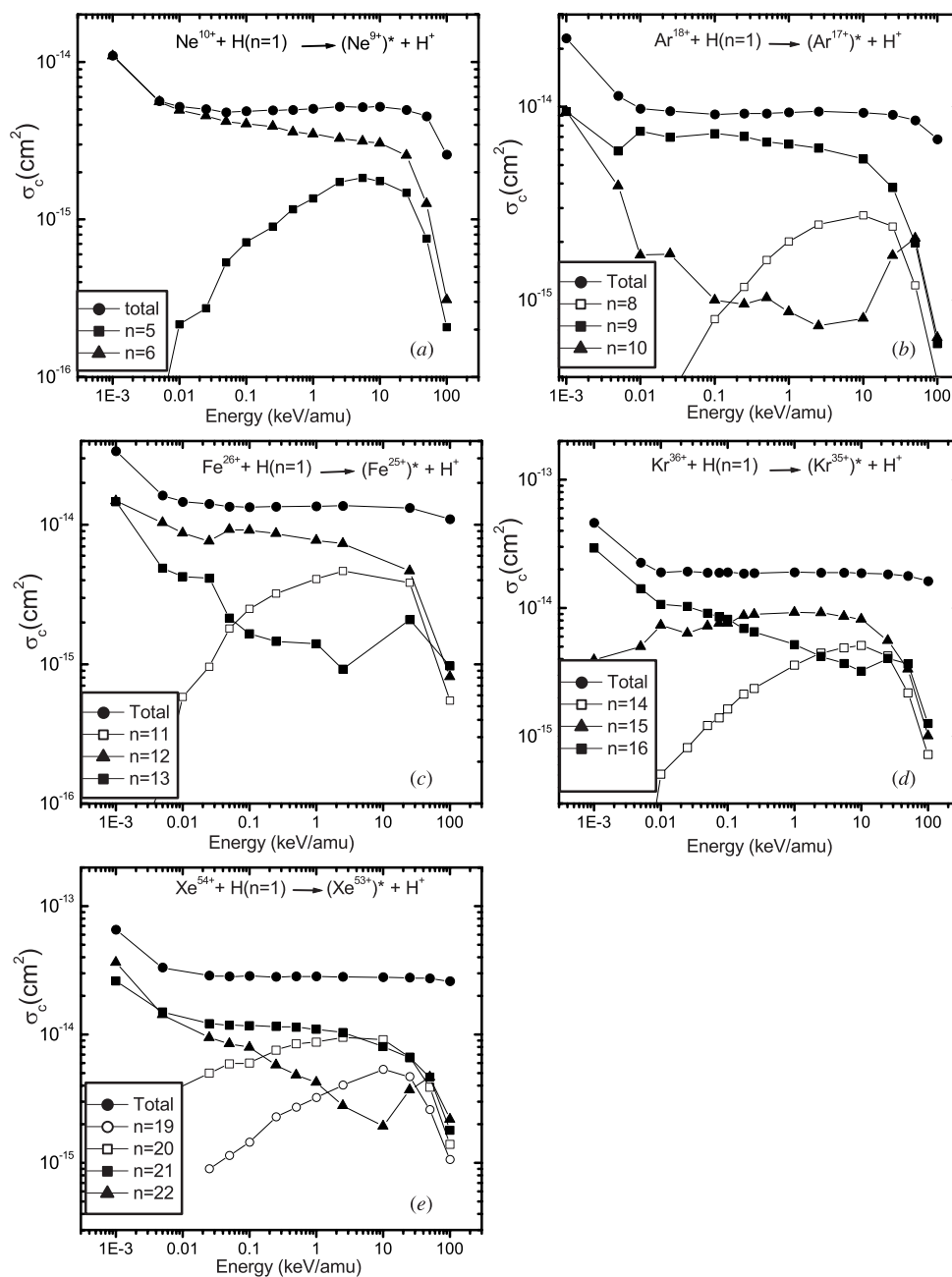


**Figure 1.** Calculated total capture cross sections and capture cross sections for the dominant  $n$  states for (a)  $\text{Ne}^{10+}$ , (b)  $\text{Ar}^{18+}$ , (c)  $\text{Fe}^{26+}$ , (d)  $\text{Kr}^{36+}$  and (e)  $\text{Xe}^{54+}$  projectile ions at collision energies ranging from  $1 \text{ eV amu}^{-1}$  to  $100 \text{ keV amu}^{-1}$ .

Statistically, capture into these high- $n$  states should produce electron orbits characterized by large  $l$  values. In figure 2 we have plotted the calculated capture cross sections for specific  $l$  values of the  $n = 6$  state of  $\text{Ne}^{10+}$  and the  $n = 16$  state of  $\text{Kr}^{36+}$ . Clearly, for collision energies

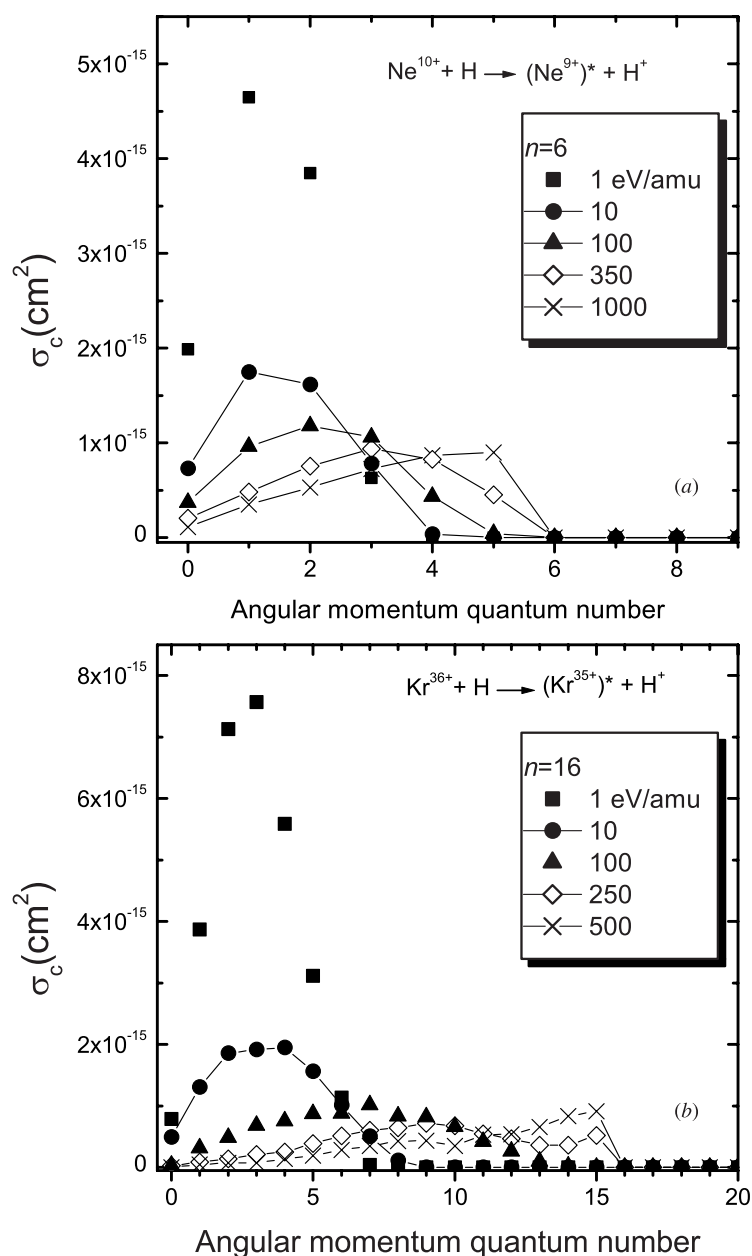


**Figure 2.** Cross sections for electron capture to specific  $l$  values by (a)  $\text{Ne}^{10+}$  (the  $n = 6$  state) at collision energies of 1, 10, 100, 350 and 1000  $\text{eV amu}^{-1}$  and by (b)  $\text{Kr}^{36+}$  (the  $n = 16$  state) at collision energies of 1, 10, 100, 250 and 500  $\text{eV amu}^{-1}$ .

of 1  $\text{keV amu}^{-1}$  for neon and 500  $\text{eV amu}^{-1}$  for krypton, the angular momentum values are statistical with  $l = 5$  and  $15$  being the most likely states populated by the captured electrons for the bare neon and krypton projectiles, respectively. It is clear that this statistical argument is not valid as one moves to lower energies. For neon we see the distribution deviating from statistical expectations for collision energies at least as high as 350  $\text{eV amu}^{-1}$ . At 100  $\text{eV amu}^{-1}$ ,  $l = 2$

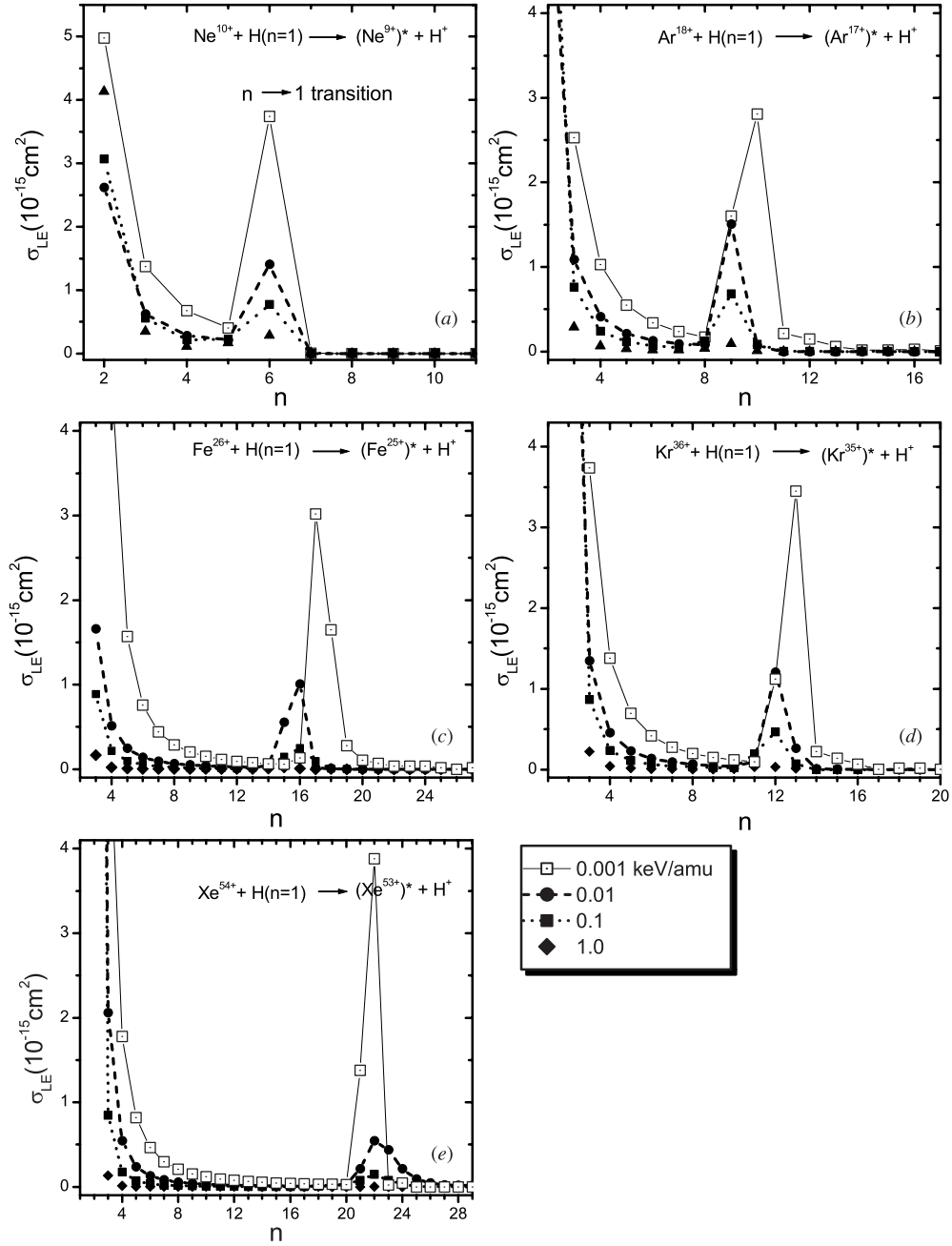


**Figure 3.** Line emission cross sections from specific  $n$  states resulting from electron capture by the projectile ions (a)  $\text{Ne}^{10+}$ , (b)  $\text{Ar}^{18+}$ , (c)  $\text{Fe}^{26+}$ , (d)  $\text{Kr}^{36+}$  and (e)  $\text{Xe}^{54+}$  at collision energies ranging from  $1 \text{ eV amu}^{-1}$  to  $1 \text{ keV amu}^{-1}$ .

is the peak value and for  $1 \text{ eV amu}^{-1}$  the peak is at  $l = 1$ . For krypton, we start to see a deviation from this statistical distribution below  $250 \text{ keV amu}^{-1}$ . At  $100 \text{ eV amu}^{-1}$  the peak value is at  $l = 7$  and at  $10$  and  $1 \text{ eV amu}^{-1}$  it is around  $l = 3$ .

The deviation from the statistical population of  $l$  values impacts the radiative decay process. At lower energies more electrons populate states with  $l = 1$ , which can decay directly to the  $n = 1, l = 0$  ground state. In figure 3 we show the CTMC results for the  $n \rightarrow 1$  K-shell x-rays emitted as a function of  $n$  for the projectile ions at collision energies of 1, 10, 100 and 1000 eV amu<sup>-1</sup>. The emission cross sections were derived using the calculated capture cross sections and a cascade matrix for radiative decay that employs hydrogenic branching ratios. We see a remarkable increase in x-rays emitted from the dominate  $n$  states for electron capture below 100 eV amu<sup>-1</sup> for each of the ions. This is a direct result of the large increase of electrons being captured into these states with  $l = 1$ .

This increase in the population of states with  $l = 1$  can be understood by noting that the initial level of the H(1s) electron is  $l = 0$ , and that angular momentum can be obtained during the collision. In the projectile rest frame  $l$  is a product of the impact parameter and the velocity of the collision (in atomic units)

$$l = b \times v. \quad (7)$$

The impact parameter,  $b$ , can be approximated by the square root of the capture cross section,  $\sigma$ , divided by  $\pi$  which scales as  $\sigma \approx 16q$ , so that

$$l \approx \sqrt{\frac{16q}{\pi}} v \quad (8)$$

predicting that the  $l = 1$  states can be populated for the ions Ne<sup>10+</sup>, Ar<sup>18+</sup>, Fe<sup>26+</sup>, Kr<sup>36+</sup> and Xe<sup>54+</sup> at collision energies less than 490, 275, 190, 140 and 90 eV amu<sup>-1</sup>, respectively. These values are consistent with the results shown in figure 2 for the neon and krypton case.

#### 4. Comparison with experiment

There is qualitative agreement between the calculated results and x-ray spectra taken at Lawrence Livermore National Laboratory using an electron beam ion trap in the magnetic trapping mode [9–11]. In this mode of operation, the electron beam is turned off and the ions are held in the trap by use of a magnetic field. This isolates charge transfer as the sole x-ray production mechanism.

Spectra recorded during the magnetic trapping mode are shown in figures 4 and 5. The first shows the emission from of Ar<sup>17+</sup> ions following the charge exchange reaction Ar<sup>18+</sup> + Ar → Ar<sup>17+(nl)</sup> + Ar<sup>+</sup>. The collision energy was 10 ± 4 eV amu<sup>-1</sup>. Strong emission from the direct decay of  $n \geq 5 \rightarrow 1$  is readily apparent. The emission from Xe<sup>53+</sup> and Xe<sup>52+</sup> ions following the charge exchange reaction Xe<sup>54+</sup> + Xe → Xe<sup>53+(nl)</sup> + Xe<sup>+</sup> and Xe<sup>53+</sup> + Xe → Xe<sup>52+(nl)</sup> + Xe<sup>+</sup>, respectively, is shown in figure 5. The collision energy in this case was 4 ± 2 eV amu<sup>-1</sup>. Again, the strong emission from the direct decay of  $n \geq 5 \rightarrow 1$  is readily apparent. The emission from Xe<sup>52+</sup> is somewhat less in energy than that of Xe<sup>53+</sup>. The reason is that the radiative decay matrix of helium-like ions differs from that of hydrogenic ions, as pointed out in [11].

The principal quantum number can be determined from the energy of the observed x-ray emission. Averaged over three independent measurements we find that the peak  $n \rightarrow 1$  K-shell emission corresponds to  $n = 9 \pm 1$  for argon and to  $n = 20 \pm 2$  for xenon. In both cases this is slightly lower than predicted by figure 3, but nevertheless in agreement within the error limits.

In figure 6 the calculated ratio of  $n \rightarrow 1$  K-shell x-rays to the  $2 \rightarrow 1$  emission has been plotted as a function of collision energy. The dramatic increase in the fraction of direct  $n \rightarrow 1$  x-ray emission becomes apparent at low energies, especially for the more highly charged ions. This energy-dependent enhancement of the direct  $n \rightarrow 1$  x-rays is in accord with the EBIT

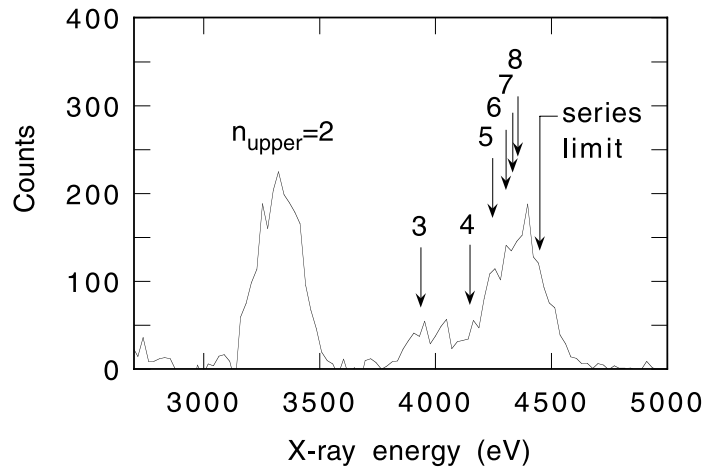


**Figure 4.**  $\text{Ar}^{17+}$  K-shell x-ray emission measured on EBIT-II following the reaction  $\text{Ar}^{18+} + \text{Ar} \rightarrow \text{Ar}^{17+}(nl) + \text{Ar}^+$ . The emission energies from specific principal quantum numbers are indicated.

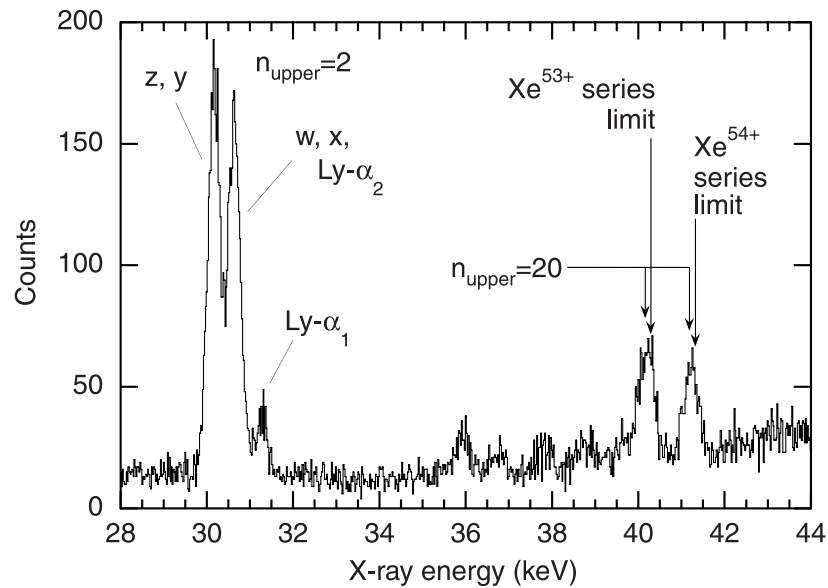


**Figure 5.**  $\text{Xe}^{54+}$  and  $\text{Xe}^{53+}$  K-shell x-ray emission measured on SuperEBIT following the reactions  $\text{Xe}^{54+} + \text{Xe} \rightarrow \text{Xe}^{53+}(nl) + \text{Xe}^+$  and  $\text{Xe}^{53+} + \text{Xe} \rightarrow \text{Xe}^{52+}(nl) + \text{Xe}^+$ . The emission energies from specific principal quantum numbers are indicated. The notation  $w$ ,  $x$ ,  $y$  and  $z$  denotes the helium-like transitions from the upper levels  $1s2p\ ^1P_1$ ,  $1s2p\ ^3P_2$ ,  $1s2p\ ^3P_1$  and  $1s2s\ ^3S_1$ , respectively.  $\text{Ly-}\alpha_1$  and  $\text{Ly-}\alpha_2$  denote the two hydrogen-like fine structure components. The background emission is due to high-energy x-rays produced by coronal discharges on the electron gun assembly, which was biased at 112 keV.

measurements for collision energies below  $10\text{ eV amu}^{-1}$ . The possible use of the energy-dependent enhancement as a powerful remote diagnostic tool to study interactions between the solar wind and cometary coma has been suggested [11].

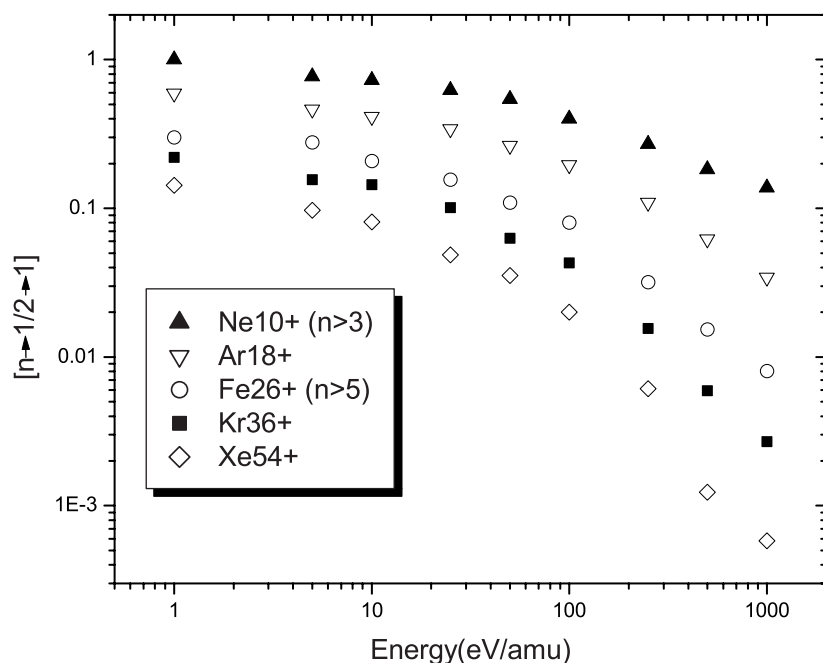


**Figure 6.** Ratio of x-rays emitted from prompt ( $np \rightarrow 1s$ ) radiative decay to ( $2p \rightarrow 1s$ ) transitions, as a function of the collision energy.

Some discrepancies between the calculations and experiments are expected due to the fact that the experiments use the neutral form of the projectile as the target. Hence, the ionization potentials change for each reaction and multiple capture can play a significant role in collisions involving the more highly charged projectiles. The CTMC calculations do not account for the role of multiple-electron capture.

## 5. Conclusion

We have used the classical trajectory Monte Carlo method to examine details of the charge transfer process between the highly charged-bare projectile ions,  $\text{Ne}^{10+}$ ,  $\text{Ar}^{18+}$ ,  $\text{Fe}^{26+}$ ,  $\text{Kr}^{36+}$  and  $\text{Xe}^{54+}$  and neutral hydrogen. At low collision energies, the capture process produces excited hydrogen-like ions with a majority of electrons being captured into one or two dominant states characterized by high principal quantum numbers. The Monte Carlo calculations show a clear deviation from the population of states with large angular momentum quantum numbers to states characterized by low values as the collision energy is lowered. These deviations begin at collision energies somewhere below  $500 \text{ eV amu}^{-1}$  depending on the ion. A result of the increase in electron capture to states with low- $l$  values is the increase in K-shell x-ray emission. Calculations predict a large increase in the fraction of prompt x-rays produced as the collision energy is lowered, and are in qualitative agreement with experimental results. Some discrepancies between the calculations and experiments are expected due to the fact that the experiments use the neutral form of the projectile as the target. Hence, the ionization potentials change for each collision, and multiple capture can play a significant role in collisions involving the more highly charged projectiles. The CTMC calculations do not account for the role of multiple-electron capture. Also, though the CTMC method has been validated for a

large number of collision systems, there is little data, either experimental or produced by other methods, with which to check the accuracy of the calculations at the low energies and large charge states involved in this work.

### Acknowledgments

This work was supported by a subcontract from the Lawrence Livermore National Laboratory. Work at the University of California Lawrence Livermore National Laboratory was carried out under the auspices of the US Department of Energy under contract no W-7405-ENG-48 and supported in part by the Office of Basic Energy Sciences of the US Department of Energy.

### References

- [1] Lisse C M *et al* 1997 *Science* **277** 1625
- [2] Isler R C 1994 *Plasma Phys. Control. Fusion* **36** 171
- [3] Synakowski E J *et al* 1995 *Phys. Rev. Lett.* **75** 3689
- [4] Cravens T E 1997 *Geophys. Res. Lett.* **24** 105
- [5] Olson R E 1981 *Phys. Rev. Lett. A* **24** 1726
- [6] Olson R E 1996 *Atomic, Molecular and Optical Physics Handbook* ed G W F Drake (New York: AIP) p 664
- [7] Olson R E, Pascale J and Hoekstra R 1992 *J. Phys. B: At. Mol. Opt. Phys.* **25** 4241
- [8] Becker R L and Mackellar A D 1984 *J. Phys. B: At. Mol. Phys.* **17** 3923
- [9] Beiersdorfer P, Schweikhard L, Crespo López-Urrutia J and Widmann K 1996 *Rev. Sci. Instrum.* **67** 3818
- [10] Beiersdorfer P, Schweikhard L, Olson R, Brown G V, Utter S B, Crespo López-Urrutia J and Widmann K 1999 *Phys. Scr. T* **80** 121
- [11] Beiersdorfer P, Olson R E, Brown G V, Chen H, Harris C L, Neill P A, Schweikhard L, Utter S B and Widmann K 2000 *Phys. Rev. Lett.* **85** 5090